Dual-Hop Underwater Optical Wireless Communication System With Simultaneous Lightwave Information and Power Transfer

Kuan Ye, Cong Zou, *Student Member, IEEE*, and Fang Yang, *Senior Member, IEEE*

***Abstract*—The most significant challenge of underwater optical wireless communication (UOWC) system is to overcome its limited coverage. To expand the achievable communication range, we investigate the performance of the dual-hop UOWC system with simultaneous lightwave information and power transfer (SLIPT). The time splitting (TS) method is adopted for wireless power transfer in the proposed system, where the information and energy are transmitted in different phases. A suitable transmission strategy is designed for the model without additional power supply, which contains three phases, i.e. information transmission, energy transmission, and forwarding process. The expressions of the average bit error rate (BER) at the target node and the energy harvested by the relay node are derived over underwater attenuation channel. Then, the effects of the TS factor and the distances on the system performance are investigated in two sub-problems, which minimize the average BER while satisfying the energy harvesting and transmitting rate constraints. Numerical results indicate the performance improvement by adopting the relay node with SLIPT.**

***Index Terms*—Underwater optical wireless communication (UOWC), simultaneous lightwave information and power transfer (SLIPT), dual-hop transmission.**

I. Introduction

In THE last few years, optical wireless communication (OWC) is considered as a promising complementary technology for radio frequency (RF) communication due to its capability of providing high data rate with low power and greater available bandwidth. Therefore, many researches have been carried out on high-speed communication of VLC under free space environment [1]–[3] and on modulation schemes [4], [5]. However, the marine environment is characterized by several distinguishing features that make it unique and different from the atmosphere environment [6]. Underwater optical wireless communication (UOWC) is expected to act as an alternative candidate in the next-generation underwater wireless communications [7], since it can deliver unprecedented high data rate with low cost and limited volume transceivers, compared to acoustic and RF methods [8], [9].

As the signal is attenuated greatly underwater with the increase of distance, the communication range of UOWC is limited. To overcome this challenge, some works focus on how to alleviate the turbulence-induced fading through spatial diversity. The bit error rate (BER) performance of multiple-input multiple-output (MIMO) UOWC systems is investigated in [10] and [11]. The channel model of MIMO UOWC systems is characterized in [12]. In [13], the channel characteristics and the BER performance of UOWC systems are studied comprehensively. In addition, some other works adopted relay-assisted technologies, which provide higher communication quality by using a relay node between the source and target nodes [14]. In [15], the BER performance of multi-hop UOWC systems under turbulence-induced fading is evaluated. The performance of relay-assisted underwater wireless optical code division multiple access networks has been investigated over turbulent channels in [16]. The performance of a hybrid RF-UWOC system is investigated in [17] where the information is transmitted to an autonomous underwater vehicle from an unmanned aerial vehicle via a relay. In [18], an Internet of Underwater Things (IoUT) collaborative system based on hybrid decoder amplification (HDAF) strategy of converged UOWC channel is studied over the aggregated lognormal fading channel. [19] investigates the performance of two-way multi-hop UOWC system with the decoder-and-forward (DF) relay. The influence of the relay on the maximum communication distance of the UOWC system is studied in [20].

Due to the fact that recharging the battery of the underwater devices is typically costly and impractical, wireless power transfer is a possible solution. In [21], a framework for the simultaneous lightwave information and power transfer (SLIPT) is proposed for the indoor VLC system. In addition, the performance optimization of the multi-cell SLIPT system serving multiple users is investigated in [22]. In addition, SLIPT has also been studied in the context of underwater environment. In [23], three SLIPT methods, namely, time switching (TS), power splitting (PS), and time switching – power splitting (TS-PS), are considered to optimize the splitting/switching factors. Simulation results validate that the proposed SLIPT methods are

Manuscript received September 2, 2021; revised September 30, 2021; accepted October 3, 2021. Date of publication October 6, 2021; date of current version October 21, 2021. This work was supported in part by the Fok Ying Tung Education Foundation, and in part by the National Natural Science Foundation of China under Grant 61871255. *(Corresponding author: Fang Yang.)*

Kuan Ye, Cong Zou, and Fang Yang are with the Department of Electronic Engineering, Beijing National Research Center for Information Science and Technology, Tsinghua University, Beijing 100084, China, and also with the Key Laboratory of Digital TV System of Guangdong Province and Shenzhen City, Research Institute of Tsinghua University, Shenzhen 518057, China (e-mail: yek19@mails.tsinghua.edu.cn; zouc19@mails.tsinghua.edu.cn; fangyang@tsinghua.edu.cn).

Digital Object Identifier 10.1109/JPHOT.2021.3118047

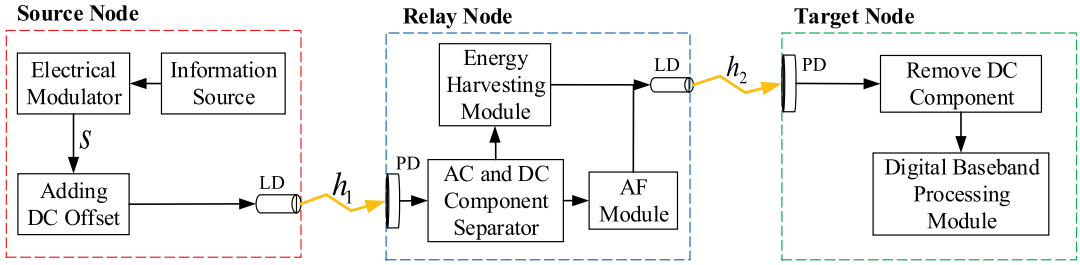

Fig. 1. Block diagram of the relaying UOWC system with SLIPT.

capable of achieving better trade-offs harvested energy versus spectral efficiency (HE-SE) region.

A major challenge for UOWC systems with SLIPT is overcoming the limited coverage. For this issue, a double-hop UOWC system with SLIPT is investigated in this paper. In the absence of additional power supply, a suitable transmission strategy is designed, which includes three stages of information transmission, energy transmission and forwarding process. Then, the effects of TS factor and distances on the system performance are studied to minimize the average BER and meet the energy collection and transmission rate constraints. In addition, Monte Carlo simulations are provided to verify the analyses of the results.

The rest of the paper is organized as follows. In Section 2, the dual-hop UOWC system with SLIPT is introduced, which is achieved by TS. The details of the transmission process are investigated in Section 3. The two sub-problems for BER minimization and position optimization are formulated and solved in Section 4. Simulation results and corresponding discussions are provided in Section 5. Finally, the paper concludes in Section 6.

II. System Model

In this paper, a relaying UOWC system with SLIPT is investigated, which consists of the source node, the relay node, and the target node. Since it is inconvenient to charge underwater and the device is expected to work for a long time, the relay node is equipped with energy harvesting devices. The proposed framework is applied in an underwater Internet-of-Thing (IoT) system, which means the transmission rate is relatively low, therefore temporal dispersion caused by scattering is not present in this case. The block diagram of the proposed system is shown in Fig. 1.

A. Transmitted Signal At the Source Node

The electrical signal corresponding to the bit stream of the information source is denoted as s with the electronic power P_e. Moreover, the peak amplitude of s is given as A, i.e. $-A \leq s \leq A$. Due to the non-negative requirement of the laser diode (LD), a direct current (DC) offset b should be added to the signal s. Therefore, the transmitted optical signal from the LD can be written as

$$x = P_o(s + b), \tag{1}$$

where P_o is the optical transmit power of the LD. The range of DC offset is given as $b \in [I_L, I_H]$, where I_L and I_H are the minimum and the maximum input bias currents, respectively. The peak amplitude should satisfy the following constraint [24]

$$A \leq \min(b - I_L, I_H - b). \tag{2}$$

Based on (1), the transmit electronic power is related to the peak amplitude of the modulated signal as [25]

$$P_e = (P_o A)^2. \tag{3}$$

B. Channel Model

The propagation of underwater beams is mainly affected by the path loss caused by absorption and dispersion, and the attenuation induced by turbulence. In this paper, these two factors are considered to model the channel.

Since the semi-collimated blue LD is adopted as the source in the proposed UOWC system, the attenuation coefficient of path loss h_{PL} is defined as [20]

$$h_{PL}(d) = d^{-2}\left(\frac{D_r}{\theta_t}\right)^2 \exp\left(-cd\left(\frac{D_r}{\theta_t d}\right)^m\right), \tag{4}$$

where c, D_r, d, θ_t, and m denote extinction coefficient, receiver aperture diameter, propagation distance, full width transmitter beam divergence angle, and correction coefficient, respectively.

The effects of turbulence are characterized by multiplying h_{PL} by a positive fading coefficient I [26]. Under the assumption of weak oceanic turbulence, I is modeled with log-normal distribution as [16]

$$f(I) = \frac{1}{2I\sqrt{2\pi\sigma^2}} \exp\left(-\frac{(\ln(I) - \mu)^2}{8\sigma^2}\right), \tag{5}$$

where μ and σ^2 are the mean and variance of the random variable $X = 0.5\ln(I)$, respectively. To ensure that the average power will not be affected by the turbulence, the fading amplitude is normalized such that $E[I] = 1$, which implies $\mu = -2\sigma^2$. Therefore, the scintillation index is given by $\sigma_I^2 = e^{4\sigma^2} - 1$.

It has been shown in [27] that channel fading due to water turbulence is negligible in the case of short time and short distance communication. In addition, according to the experimental results in [28], the value of scintillation index is very small (lower than 0.02) under the communication distance considered in this paper, which means that the fluctuation of I is little. Thus the effects of turbulence are approximated by the mean value of I.

The total channel attenuation coefficient h can then be given by

$$h(d) = \bar{I} h_{PL}(d). \tag{6}$$

Besides the assumption that the wavelength of light remains constant throughout the communication, the same receiving devices are used at the relay node and the source node. Therefore, the attenuation coefficients between the source node and the relay node, the relay node and the target node can be respectively given as

$$h_1 = h(d_1), h_2 = h(d_2), \tag{7}$$

where d_1 and d_2 denote the source-to-relay and relay-to-target distances, respectively.

C. Transmission Strategy

An amplify-and-forward (AF) relay node with energy harvesting devices is adopted in the proposed UOWC system. Due to the utilization of the TS transmission strategy and the relay node, the communication process is divided into three phases, i.e. Phase I, Phase II, and Phase III, which denote information transmission, energy transmission and forwarding process, respectively.

On-off keying (OOK) is adopted as the modulation technique. Consider a block-based transmission between the source and relay nodes with duration T where each block contains N OOK symbols with symbol period T_s, i.e., $T = NT_s$. The TS factor β is introduced due to the TS strategy, which means that the proportion of time transmitting information is $T_1 = \beta T$. Consequently, the duration of time $T_2 = (1-\beta)T$ is dedicated for energy harvesting. And the duration of relay-to-target communication is set to be the same as that of Phase I, i.e. $T_3 = T_1$, which ensures that the transmission symbol rate remains unchanged throughout the whole communication.

As mentioned before, the transmission process is divided into three phases. In Phase I, the source node sends the signal x to the relay node in duration T_1. Then, the received signal y_1 at the relay node is given by $y_1 = \eta h_1 x + n_1$, where η is the photodetector (PD) responsivity and n_1 denotes the additive white Gaussian noise (AWGN) at the relay node. Let A_1 and A_2 respectively denote the peak amplitude of s in Phase I and Phase II, which are given by $A_1 = (I_H - I_L)/2$ and $A_2 = 0$. Therefore, the values of the DC offset during the two phases are given as $b_1 = (I_H + I_L)/2$ and $b_2 = I_H$, respectively. Based on the foregoing analysis, the energy harvested by the relay node is formulated as [21]

$$E_r = \eta f P_o h_1 V_t T(1-\beta) b_2 \ln\left(1 + \frac{\eta P_o h_1 b_2}{I_0}\right), \tag{8}$$

where f is the fill factor, V_t is the thermal voltage, and I_0 is the dark saturation current of the PD.

In Phase III, the relay node forwards the signal y_1 to the target node with all the collected energy. Thus, the total power budget P_r of the relay node in Phase III can be written as

$$P_r = \frac{E_r}{T_3} = \left(\frac{1}{\beta} - 1\right) \eta f P_o h_1 V_t b_2 \ln\left(1 + \frac{\eta P_o h_1 b_2}{I_0}\right). \tag{9}$$

Then, the transmitted signal at the relay node is given by

$$x_r = Z y_1, \tag{10}$$

where $Z = \sqrt{P_r/[(\eta h_1)^2(P_e + b_1^2) + \sigma_1^2]}$. After Phase III, the signal received by the target node can be expressed as $y_2 = \eta h_2 x_r + n_2$, where n_2 denotes the AWGN at the target node. Therefore, the source-to-target signal-to-noise ratio (SNR) can be given as

$$\gamma = \frac{(\eta^2 h_1 h_2 Z P_o A_1)^2 ||s||_2^2}{((\eta h_2 Z)^2 \sigma_1^2 + \sigma_2^2) N}, \tag{11}$$

where σ_1^2 and σ_2^2 denote the variances of n_1 and n_2, respectively.

The BER for OOK over real AWGN channel is given by [29]

$$BER = Q\left(\eta h_1 P_o A_1 ||s||_2 \sqrt{\frac{(\eta h_2 Z)^2}{2N[(\eta h_2 Z)^2 \sigma_1^2 + \sigma_2^2]}}\right). \tag{12}$$

Note that the receiver of the relay node works in information decoding mode for a duration of $T_1 = \beta T$. Taking a time average for the SLIPT strategy, the BER is obtained as [30], [31]

$$BER_t = \beta BER. \tag{13}$$

III. Problem Formulation and Solution

According to (4) and (13), the system performance is affected by both the distances and the TS factor. Therefore, two sub-problems are proposed to investigate the effects of these elements in this section.

A. BER Optimization

The values of these parameters d_1, and d_2 are fixed in this subsection. In this case, our goal is to minimize the average BER at the target node, subject to the minimum harvested energy requirements and data rate constraints. The corresponding optimization problem is formulated and optimally solved in this subsection.

Considering the fact that maintaining a certain transmission rate is needed in the communication process, a data rate threshold R_{th} should be set. Let R_b denote the rate at which the source node sends the information, then the equivalent communication rate between the source and the relay nodes is $\overline{R} = \beta R_b$ for the SLIPT scheme. Mathematically, the BER optimization problems for TS can be formulated as

$$\min_{\beta} \quad BER_t \tag{14a}$$

$$s.t. \quad E_r \geq E_{th}, \tag{14b}$$

$$\overline{R} \geq R_{th}, \tag{14c}$$

$$0 \leq \beta \leq 1, \tag{14d}$$

where E_{th} denotes the harvested energy threshold of the relay node.

Let $K_1 = \eta f P_o h_1 V_t T b_2 \ln(1 + \eta P_o h_1 b_2 / I_0)$. The first derivative of E_r with respect to β is given as

$$\frac{\partial E_r}{\partial \beta} = -K_1. \tag{15}$$

Due to $K_1 > 0$, E_r is decreasing with respect to β. Considering the inequalities in (14b), the value range of β is formulated as

$$\beta \leq 1 - \frac{E_{th}}{K_1}. \tag{16}$$

In addition, considering the inequalities in (14c), it can be derived that

$$\beta \geq \frac{R_{th}}{R_b}. \tag{17}$$

Using the approximation $Q(x) \approx (1/12)\exp(-x^2/2) + (1/4)\exp(-2x^2/3)$ [32], (13) can be rewritten as

$$BER_t \approx \beta\left(\frac{1}{12}e^{-\frac{\gamma}{4}} + \frac{1}{4}e^{-\frac{\gamma}{3}}\right). \tag{18}$$

Then, the first derivative of BER_t with respect to β is formulated as

$$\frac{\partial BER_t}{\partial \beta} = \frac{1}{12}e^{-\frac{\gamma}{4}} + \frac{1}{4}e^{-\frac{\gamma}{3}} - \left(\frac{1}{48}e^{-\frac{\gamma}{4}} + \frac{1}{12}e^{-\frac{\gamma}{3}}\right)\beta\frac{d\gamma}{d\beta}. \tag{19}$$

Given a definition of $K_2 = (\eta h_1)^2(P_e + b_1^2) + \sigma_1^2$, the expression in (11) can be rewritten as

$$\gamma = \frac{(\eta^2 h_1 h_2 P_o A_1)^2}{(\eta h_2)^2\sigma_1^2 + \sigma_2^2/Z^2} = \frac{(\eta^2 h_1 h_2 P_o A_1)^2}{(\eta h_2)^2\sigma_1^2 + K_2\sigma_2^2/P_r}. \tag{20}$$

It is obvious that P_r is decreasing with respect to β according to (9). Therefore, it can be deduced that γ decreases with the increase of β, i.e. $d\gamma/d\beta < 0$. Based on this conclusion, we have $\partial BER_t/\partial\beta > 0$, which means BER_t is increasing with respect to β. Thus, the optimal value of β in (13) is given by

$$\beta^* = \frac{R_{th}}{R_b}, \tag{21}$$

where $(\cdot)^*$ denotes optimality.

B. Position Optimization

The value of the parameter β is fixed in this subsection. Under the assumption that the position of the relay node is on a line between the source and the target nodes, let L denote the distance from the source node to target node, i.e. $L = d_1 + d_2$. In this case, our goal is to minimize the average BER at the target node by finding the optimal position of the relay node.

According to (18), minimization of source-to-target BER is equivalent to maximizing source-to-target SNR. The value of $\sigma_1^2\sigma_2^2$ is negligible, therefore the expression of γ in (20) can be approximated as

$$\gamma = \frac{(\eta h_1 h_2 P_o A_1)^2 P_r}{h_2^2\sigma_1^2 P_r + h_1^2(P_e + b_1^2)\sigma_2^2}. \tag{22}$$

Replacing (4) and (7) in (22), the source-to-target SNR can then be rewritten as

$$\gamma = \frac{C_1 u(d_1)[g(d_1)]^2 \ln[1 + C_3 q(d_1)]}{C_2 g(d_1)\ln[1 + C_3 q(d_1)] + C_4 q(d_1)}, \tag{23}$$

where

$$C_1 = \left(\frac{1}{\beta} - 1\right)\eta^3 P_o^3 A_1^2 f V_t b_2 \left(\frac{D_r}{\theta_t}\right)^{10}, \tag{24}$$

$$C_2 = \left(\frac{1}{\beta} - 1\right)\eta\sigma_1^2 P_o f V_t b_2 \left(\frac{D_r}{\theta_t}\right)^4, \tag{25}$$

$$C_3 = \frac{\eta P_o b_2}{I_0}\left(\frac{D_r}{\theta_t}\right)^2, \tag{26}$$

$$C_4 = (P_e + b_1^2)\sigma_2^2\left(\frac{D_r}{\theta_t}\right)^4, \tag{27}$$

$$q(d_1) = d_1^{-2} e^{-c(\frac{D_r}{\theta_t})^m d_1^{1-m}}, \tag{28}$$

$$u(d_1) = d_1^{-4} e^{-2c(\frac{D_r}{\theta_t})^m d_1^{1-m}}, \tag{29}$$

$$g(d_1) = (L - d_1)^{-2} e^{-c(\frac{D_r}{\theta_t})^m (L-d_1)^{1-m}}, \tag{30}$$

respectively. It can be seen that $u(d_1) = [q(d_1)]^2$, hence $u'(d_1) = 2q(d_1)q'(d_1)$. After taking the derivative of (23) and setting it to zero, a complicated equation is derived. And then by proper approximation, the equation can be simplified as

$$\begin{aligned} &2C_2 q'(d_1)[g(d_1)]^3 \ln[1 + C_3 q(d_1)] + C_4 q(d_1) \\ &[q'(d_1)g(d_1) + 2q(d_1)g'(d_1)] = 0, \end{aligned} \tag{31}$$

where

$$\begin{aligned} q'(d_1) = &-c(1-m)\left(\frac{D_r}{\theta_t}\right)^m d_1^{-m-2} e^{-c\left(\frac{D_r}{\theta_t}\right)^m d_1^{1-m}} \\ &- 2d_1^{-3} e^{-c\left(\frac{D_r}{\theta_t}\right)^m d_1^{1-m}}, \end{aligned} \tag{32}$$

$$g'(d_1) = -q'(L - d_1). \tag{33}$$

The approximation made in the derivation process will be verified in the simulation part. It is difficult to give a closed-form expression of d_1 due to the complexity of (31), however the numerical solution can be easily obtained via MATLAB.

IV. Simulation Result and Discussion

In this section, the simulation results consist of three parts, one of which is the verification of some approximations in the derivation process. The second part is the Monte Carlo simulation to verify the correctness of the BER. The rest part is to demonstrate the performance of the proposed UOWC system through numerical results, considering different water types and system parameters. Unless stated otherwise, the simulation parameters are given in Table I.

The corresponding relationship between D_r, θ_t, and m can be found in [20]. In order to illustrate the effectiveness of the solution in (31), the comparison between the optimal position (OP) and the exact maximum of γ is presented in Fig. 2 and Fig. 3, where $D_r = 20$ cm, $\theta_t = 6^\circ$, and $m = 0.21$ in Fig. 2. It is observed that the difference between OP and the maximum point is negligible, therefore the simplified equation in (31) is very important to save computational effort while maintaining accuracy. In general, the optimal solution performs well in all conditions we have considered.

The impacts of L and water types on BER are shown in Fig. 4, where $D_r = 5$ cm and $\theta_t = 6^\circ$. It can be seen that there is little difference between the simulation results and theoretical values, when the BER threshold is 10^{-6} in clear ocean and coastal ocean.

TABLE I
SIMULATION PARAMETERS AND VALUES

Parameter	Symbol	Value
PD responsivity	η	0.4 A/W
Minimum input bias current	I_L	25 mA
Maximum input bias current	I_H	45 mA
Fill factor	f	0.75
LD power	P_o	30 W/A
Thermal voltage	V_t	25 mV
Dark saturation current	I_0	10^{-9} A
Variances of n_1	σ_1^2	10^{-14}
Variances of n_2	σ_2^2	10^{-14}
Data rate	R_b	1 Mbps

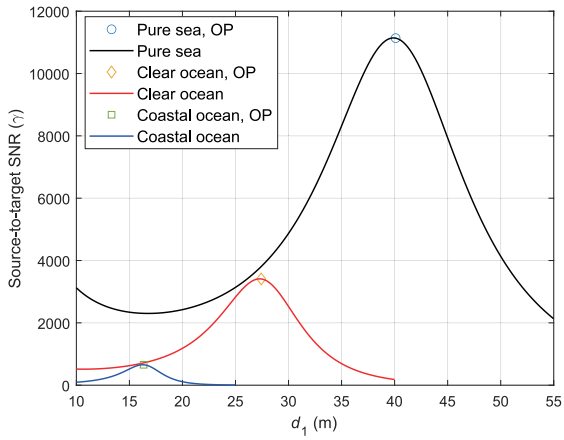

Fig. 2. Comparison between OP and exact maximum for different water types.

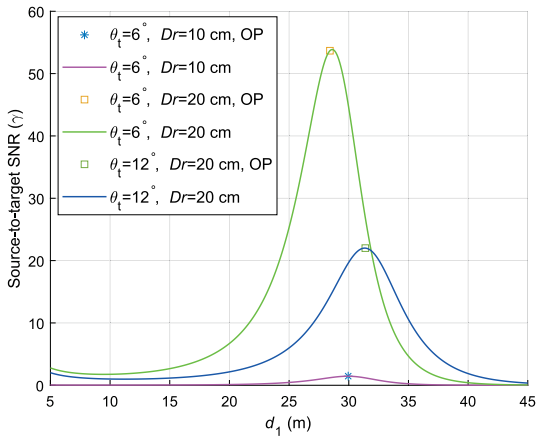

Fig. 3. Comparison between OP and exact maximum for different D_r and θ_t.

The impacts of the transmission power P_o and D_r on BER are shown in Fig. 5, where $\theta_t = 6^\circ$ and the water type is coastal ocean. It is observed that, the simulation curve is consistent with the theoretical one, when $D_r = 5$ cm and $D_r = 10$ cm. Due to the large amount of data, only the mean of the results of the three experiments was taken, hence there may be some accidental errors that lead to these small differences.

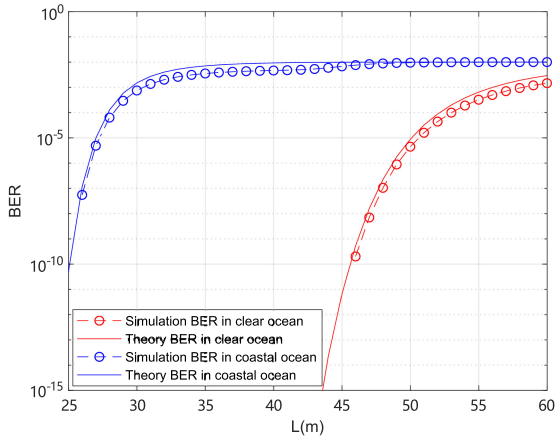

Fig. 4. Comparison of simulation and theory results in different water types.

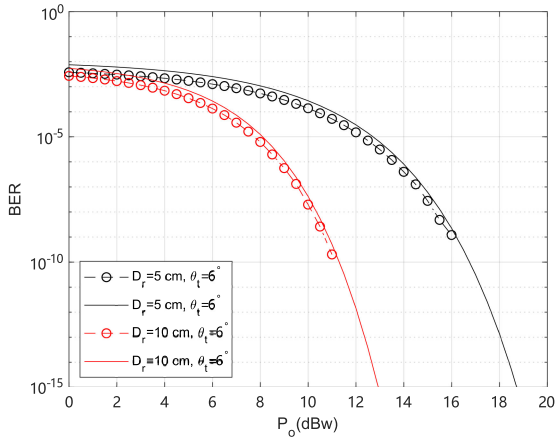

Fig. 5. Comparison of simulation and theory results for different receiver aperture sizes.

The impact of β on BER_t is shown in Fig. 6, where the extinction coefficients are respectively given by $c = 0.056\,\mathrm{m}^{-1}$, $0.150\,\mathrm{m}^{-1}$, and $0.399\,\mathrm{m}^{-1}$ for pure sea, clear ocean, and coastal ocean [33]. The transmission distances of lightwave vary in different water types, hence L is set to be 30 m, 50 m, and 80 m for coastal ocean, clear ocean, and pure sea, respectively. The performance when the relay node is placed at the OP is compared with that when the relay node is set equidistant (ED), i.e. $d_1 = d_2$. It can be seen that the system with OP relay node has better performance whatever the water type is. For example, when β is given as 0.02, the BER_t in coastal ocean with OP relay node is 1.5×10^{-8}. This increases to 2.5×10^{-4} for coastal ocean with ED relay node. It can also be noted that the average BER performance of the system can be improved by reducing β, which means that the communication rate is sacrificed to increase the harvested energy.

In Fig. 7, the average BER performance of system with relay node is compared to that without relay node for different receiver aperture sizes. Coastal ocean, $\theta_t = 6^\circ$, and $\beta = 0.02$ are considered in this case. It can be found that when $D_r = 5\,\mathrm{cm}$, $D_r = 10$ cm, and $D_r = 20$ cm, the system with relay node has better

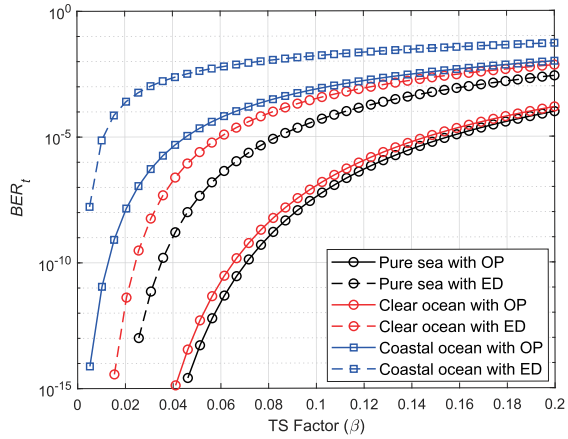

Fig. 6. BER_t versus β for different water types.

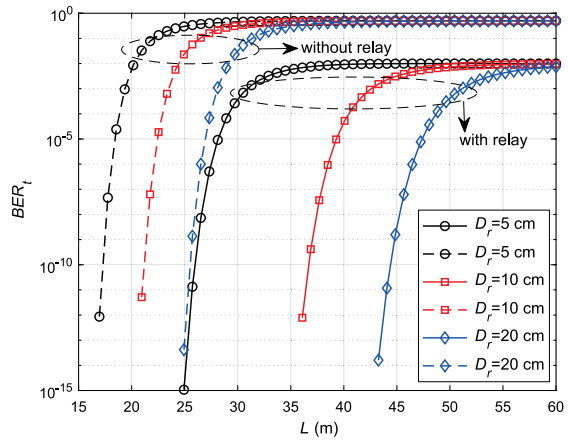

Fig. 7. Effect of the relay node on BER_t in coastal ocean for different receiver aperture sizes.

performance than that without, which means the problem of fast signal attenuation can be effectively solved by adopting relay node, so as to expand the communication distance. For example, given $D_r = 5$ cm and the BER requirement is 10^{-6}, the distance that the system with relay node can achieve is 27.4 m, which decreases to 18.1 m for the system without relay node. Moreover, it is also found that as the receiver aperture size increases, the system performance is improved since the relay node can harvest more energy while the attenuation is lower. In Fig. 8, the effect of the relay node is investigated in coastal ocean for different beam divergence angles and the receiver aperture size is fixed to 20 cm. It is observed that when $\theta = 6°$, $\theta = 12°$, and $\theta = 18°$, adopting the relay node can improve the system performance greatly. For example, when θ_t and the BER requirement are respectively given as $6°$ and 10^{-6}, the system with relay node can communicate at a distance of 41.5 m, which decreases to 26.4 m for the system without relay node. In addition, it can also be seen that with the increase of beam divergence angle, the average BER performance of system gradually declines, since some photons may not be received, resulting in less energy being collected by the relay node.

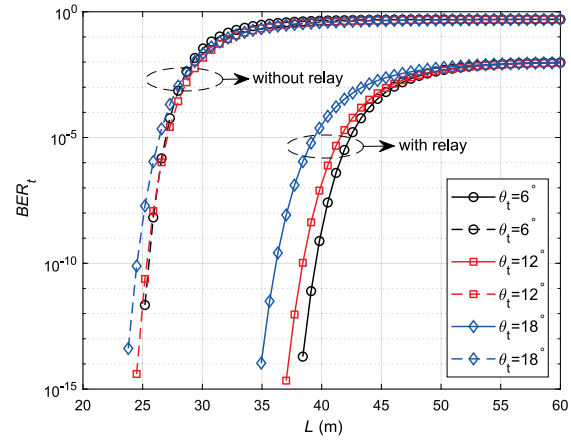

Fig. 8. Effect of the relay node on BER_t in coastal ocean for different beam divergence angles.

V. Conclusion

In this paper, a dual-hop structure with SLIPT has been proposed for the UOWC system based on TS transmission strategy. The communication process is divided into three phases, due to the utilization of the TS scheme and the half-duplex property of the relay node. Two sub-problems are established via investigating the details of the transmission process. Then, the TS factor and relay position are determined by solving these problems. Moreover, our simulation results confirmed that the employment of the relay node is important for UOWC system to expand the communication distance.

References

[1] Y. Wang, L. Tao, X. Huang, J. Shi, and N. Chi, "8-Gb/s RGBY LED-based WDM VLC system employing high-order CAP modulation and hybrid post equalizer," *IEEE Photon. J.*, vol. 7, no. 6, Aug. 2015, Art. no. 7904507.

[2] C.-H. Yeh *et al.*, "1.7 to 2.3 Gbps OOK LED VLC transmission based on 4×4 color-polarization-multiplexing at extremely low illumination," *IEEE Photon. J.*, vol. 11, no. 4, Aug. 2019, Art. no. 7904206.

[3] I.-C. Lu, C.-H. Yeh, D.-Z. Hsu, and C.-W. Chow, "Utilization of 1-GHz VCSEL for 11.1-Gbps OFDM VLC wireless communication," *IEEE Photon. J.*, vol. 8, no. 3, Jun. 2016, Art. no. 7904106.

[4] Y. Sun, F. Yang, and J. Gao, "Comparison of hybrid optical modulation schemes for visible light communication," *IEEE Photon. J.*, vol. 9, no. 3, Jun. 2017, Art. no. 7904213.

[5] Y. Sun, F. Yang, and L. Cheng, "An overview of OFDM-based visible light communication systems from the perspective of energy efficiency versus spectral efficiency," *IEEE Access*, vol. 6, pp. 60824–60833, Oct. 2018.

[6] M. Jouhari, K. Ibrahimi, H. Tembine, and J. Ben-Othman, "Underwater wireless sensor networks: A survey on enabling technologies, localization protocols, and Internet of Underwater Things," *IEEE Access*, vol. 7, pp. 96879–96899, Jul. 2019.

[7] N. Chi and M. Shi, "Enabling technologies for high-speed LED based underwater visible light communications," in *Proc. IEEE Int. Conf. Signal Process. Commun. Comput.*, 2019, pp. 1–4.

[8] X. Liu *et al.*, "Laser-based white-light source for high-speed underwater wireless optical communication and high-efficiency underwater solid-state lighting," *Opt. Exp.*, vol. 26, no. 15, pp. 19259–19274, Jul. 2018.

[9] P. K. Sajmath, R. V. Ravi, and K. K. A. Majeed, "Underwater wireless optical communication systems: A survey," in *Proc. 7th Int. Conf. Smart Structures Syst.*, 2020, pp. 1–7.

[10] M. V. Jamali and J. A. Salehi, "On the BER of multiple-input multiple-output underwater wireless optical communication systems," in *Proc. 4th Int. Workshop Opt. Wireless Commun.*, 2015, pp. 26–30.

[11] M. V. Jamali, J. A. Salehi, and F. Akhoundi, "Performance studies of underwater wireless optical communication systems with spatial diversity: MIMO scheme," *IEEE Trans. Commun.*, vol. 65, no. 3, pp. 1176–1192, Mar. 2017.

[12] H. Zhang and Y. Dong, "Impulse response modeling for general underwater wireless optical MIMO links," *IEEE Commun. Mag.*, vol. 54, no. 2, pp. 56–61, Feb. 2016.

[13] M. V. Jamali, P. Nabavi, and J. A. Salehi, "MIMO underwater visible light communications: Comprehensive channel study, performance analysis, and multiple-symbol detection," *IEEE Trans. Veh. Technol.*, vol. 67, no. 9, pp. 8223–8237, Sep. 2018.

[14] W. Liu, J. Ding, J. Zheng, X. Chen, and C. L. I, "Relay-assisted technology in optical wireless communications: A survey," *IEEE Access*, vol. 8, pp. 194384–194409, Oct. 2020.

[15] M. V. Jamali, A. Chizari, and J. A. Salehi, "Performance analysis of multi-hop underwater wireless optical communication systems," *IEEE Photon. Technol. Lett.*, vol. 29, no. 5, pp. 462–465, Mar. 2017.

[16] M. V. Jamali, F. Akhoundi, and J. A. Salehi, "Performance characterization of relay-assisted wireless optical CDMA networks in turbulent underwater channel," *IEEE Trans. Wireless Commun.*, vol. 15, no. 6, pp. 4104–4116, Feb. 2016.

[17] S. Li, L. Yang, D. B. Da Costa, and S. Yu, "Performance analysis of UAV-based mixed RF-UWOC transmission systems," *IEEE Trans. Commun.*, vol. 69, no. 8, pp. 5559–5572, Aug. 2021.

[18] S. Li, P. Wang, W. Pang, W. Wang, and L. Guo, "Performance analysis for cooperative communication system in optical IoUT network with HDAF strategy," *IEEE Photon. J.*, vol. 13, no. 3, Jun. 2021, Art. no. 7300422.

[19] F. Xing, H. Yin, and L. Jing, "Performance characterization of two-way multi-hop underwater networks in turbulent channels," *Chin. Opt. Lett.*, vol. 17, no. 10, Oct. 2019, Art. no. 100005.

[20] M. Elamassie, F. Miramirkhani, and M. Uysal, "Performance characterization of underwater visible light communication," *IEEE Trans. Wireless Commun.*, vol. 67, no. 1, pp. 543–552, Jan. 2019.

[21] P. D. Diamantoulakis, G. K. Karagiannidis, and Z. Ding, "Simultaneous lightwave information and power transfer (SLIPT)," *IEEE Trans. Green Commun.*, vol. 2, no. 3, pp. 764–773, Sep. 2018.

[22] A. M. Abdelhady, O. Amin, B. Shihada, and M. Alouini, "On the optimization of multi-cell SLIPT systems," in *Proc. IEEE Glob. Commun. Conf.*, 2018, pp. 1–6.

[23] M. Uysal, S. Ghasvarianjahromi, M. Karbalayghareh, P. D. Diamantoulakis, G. K. Karagiannidis, and S. M. Sait, "SLIPT for underwater visible light communications: Performance analysis and optimization," *IEEE Trans. Commun.*, to be published, doi: 10.1109/TWC.2021.3076159.

[24] T. Rakia, H. Yang, F. Gebali, and M. Alouini, "Optimal design of dual-hop VLC/RF communication system with energy harvesting," *IEEE Commun. Lett.*, vol. 20, no. 10, pp. 1979–1982, Jul. 2016.

[25] M. Obeed, H. Dahrouj, A. M. Salhab, S. A. Zummo, and M.-S. Alouini, "DC-bias and power allocation in cooperative VLC networks for joint information and energy transfer," *IEEE Trans. Wireless Commun.*, vol. 18, no. 12, pp. 5486–5499, Dec. 2019.

[26] S. M. Navidpour, M. Uysal, and M. Kavehrad, "BER performance of free-space optical transmission with spatial diversity," *IEEE Trans. Commun.*, vol. 6, no. 8, pp. 2813–2819, Aug. 2007.

[27] F. Hanson and M. Lasher, "Effects of underwater turbulence on laser beam propagation and coupling into single-mode optical fiber," *Appl. Opt.*, vol. 49, no. 16, pp. 3224–3230, Jun. 2010.

[28] H. Gerçekcioğlu, "Bit error rate of focused gaussian beams in weak oceanic turbulence," *J. Opt. Soc. Amer. A*, vol. 31, no. 9, pp. 1963–1968, Sep. 2014.

[29] J. Grubor, S. Randel, K. Langer, and J. W. Walewski, "Broadband information broadcasting using LED-based interior lighting," *J. Lightw. Technol.*, vol. 26, no. 24, pp. 3883–3892, Dec. 2008.

[30] H. G. Sandalidis, A. Vavoulas, T. A. Tsiftsis, and N. Vaiopoulos, "Illumination, data transmission, and energy harvesting: The three-fold advantage of VLC," *Appl. Opt.*, vol. 56, no. 12, pp. 3421–3427, Apr. 2017.

[31] S. Ghasvarianjahromi, M. Karbalayghareh, P. D. Diamantoulakis, G. K. Karagiannidis, and M. Uysal, "Simultaneous lightwave information and power transfer in underwater visible light communications," in *Proc. IEEE 30th Annu. Int. Symp. Pers., Indoor Mobile Radio Commun.*, 2019, pp. 1–6.

[32] M. Chiani, D. Dardari, and M. K. Simon, "New exponential bounds and approximations for the computation of error probability in fading channels," *IEEE Trans. Wireless Commun.*, vol. 2, no. 4, pp. 840–845, Jul. 2003.

[33] H. Kaushal and G. Kaddoum, "Underwater optical wireless communication," *IEEE Access*, vol. 4, pp. 1518–1547, Apr. 2016.